ChemPubSoc Europe

DOI: 10.1002/ejic.201501143

EurJIC European Journal of Inorganic Chemistry

Full Paper

Phosphors

Syntheses, Crystal Structures, NMR Spectroscopy, and Vibrational Spectroscopy of $Sr(PO_3F)\cdot H_2O$ and $Sr(PO_3F)$

Stephan G. Jantz,[a] Leo van Wüllen,[b] Andreas Fischer,[b] Eugen Libowitzky,[c] Enrique J. Baran,[d] Matthias Weil,*[e] and Henning A. Höppe*[a]

Abstract: Single crystals of $Sr(PO_3F)\cdot H_2O$ {$P2_1/c$, $Z = 4$, $a = 7.4844(2)$ Å, $b = 7.0793(2)$ Å, $c = 8.4265(2)$ Å, $\beta = 108.696(1)°$, $V = 422.91(2)$ Å^3, 2391 F_o^2, 70 parameters, $R_1[F^2 > 2\sigma(F^2)] = 0.036$; $wR_2(F^2$ all) = 0.049, $S = 1.054$} were grown from an aqueous solution by a metathesis reaction. The structure comprises $[SrO_8]$ polyhedra and PO_3F tetrahedra that form a layered arrangement parallel to (100). The topotactic dehydration of this phase proceeds between 80 and 140 °C to afford $Sr(PO_3F)$. The monazite-type crystal structure of $Sr(PO_3F)$ was elucidated from the X-ray powder data by simulated annealing [$P2_1/c$, $Z = 4$, $a = 6.71689(9)$ Å, $b = 7.11774(11)$ Å, $c = 8.66997(13)$ Å, $\beta = 128.0063(7)°$, $V = 326.605(8)$ Å^3, $R_p = 0.010$, $R_{wp} = 0.015$, $R_F = 0.030$]. During dehydration, the structure of $Sr(PO_3F)\cdot H_2O$ collapses along [100] from a layered arrangement into a framework structure, accompanied by a change of the coordination number of the Sr^{2+} ions from eight to nine. The magic-angle spinning (MAS) NMR and vibrational spectroscopy data of both phases are discussed.

Introduction

In the course of our investigations of silicate-analogous materials[1–8] focussing on alkaline-earth compounds as potential host structures for doping with divalent europium or manganese ions for application as phosphors, we started a systematic study of the crystal structures of substituted phosphates $(PO_3X)^{m-}$ (X = S, $m = 3$; X = F, $m = 2$). For instance, we clarified the chemical and crystallographic properties of the monothiophosphates $NaM(PO_3S)\cdot 9H_2O$ (M = Mg, Ca, Ba),[1,7] which are subject to decomposition at relatively low temperatures owing to the evaporation of H_2S. Although thio derivatives with the $(PO_3S)^{3-}$ anion would provide a softer coordination environment for luminescent inner or outer transition-metal ions, fluorido derivatives with the $(PO_3F)^{2-}$ anion should act as harder ligands in the sense of the hard and soft acids and bases (HSAB) concept.[9] Therefore, by this approach, the emission of structure dopant Eu^{2+} ions can be tuned accordingly.

Monofluorophosphates are isoelectronic with the corresponding sulfates; they are interesting owing to their high technological relevance, for example, as toothpaste additives, active agents during the biomineralisation of fluoroapatite, solubility inhibitors for lead in potable water sources, wood preservatives or corrosion inhibitors.[2] In systematic studies devoted to structure determinations and solid-state NMR investigations of monofluorophosphates with closed-shell d^{10} metal cations, we have so far elucidated the properties of $Ag_2(PO_3F)$,[10] $Hg_2(PO_3F)$[11] and $Ba(PO_3F)$.[2] In addition to that of $Ba(PO_3F)$, the crystal structure of another alkaline-earth representative, namely, $Ca(PO_3F)\cdot 2H_2O$, has already been determined.[12] For $Sr(PO_3F)\cdot H_2O$, various preparation methods towards polycrystalline samples as well as their thermal behaviour have been reported;[13–17] with respect to structural data, only a set of lattice parameters was given.[17]

In this contribution, we report the syntheses and crystal structures of $Sr(PO_3F)\cdot H_2O$ and its intermediate thermal decomposition product $Sr(PO_3F)$. To unequivocally show the presence of P–F bonds, to exclude the presence of P–OH bonds and to prove a possible O/F ordering in the tetrahedral $(PO_3F)^{2-}$ anions, which is difficult to derive solely from X-ray diffraction experiments, we also included careful solid-state NMR and vibrational spectroscopy studies. Electrostatic calculations based on the Madelung part of lattice energy (MAPLE) concept confirmed the spectroscopic and diffraction data.

Results and Discussion

Crystal Structure of $Sr(PO_3F)\cdot H_2O$

Strontium monofluorophosphate hydrate, $Sr(PO_3F)\cdot H_2O$ (**1**), crystallises in a new structure type in the monoclinic space

[a] *Lehrstuhl für Festkörperchemie, Institut für Physik, Universität Augsburg, Universitätsstr. 1, 86159 Augsburg, Germany*
E-mail: henning.hoeppe@physik.uni-augsburg.de
http://www.ak-hoeppe.de
[b] *Lehrstuhl für Chemische Physik und Materialwissenschaften, Institut für Physik, Universität Augsburg, Universitätsstr. 1, 86159 Augsburg, Germany*
[c] *Institute for Mineralogy and Crystallography, Faculty of Geosciences, Geography and Astronomy, University of Vienna, Althanstr. 14, 1090 Vienna, Austria*
[d] *Centro de Quimica Inorganica (CEQUINOR/CONICET, UNLP), Facultad de Ciencias Exactas, Universidad Nacional de La Plata, C. Correo 962, 1900 La Plata, Argentina*
[e] *Institute for Chemical Technologies and Analytics, Division Structural Chemistry, Vienna University of Technology, Getreidemarkt 9/164-SC, 1060 Vienna, Austria*
E-mail: matthias.weil@tuwien.ac.at
http://www.cta.tuwien.ac.at/sc/experimental_solid_state_chemistry/
Supporting information and ORCID(s) from the author(s) for this article are available on the WWW under http://dx.doi.org/10.1002/ejic.201501143.

group $P2_1/c$. All of the atoms in the asymmetric unit occupy positions on Wyckoff site 4*e*. The Sr^{2+} cations are arranged in zigzag chains running parallel to [001] with Sr–Sr distances of 4.47 Å. The fluorophosphate anions are aligned in rows along the same direction with alternating orientations (up or down) of the PO_3F tetrahedra with P–P distances of 4.44 Å (Figure 1).

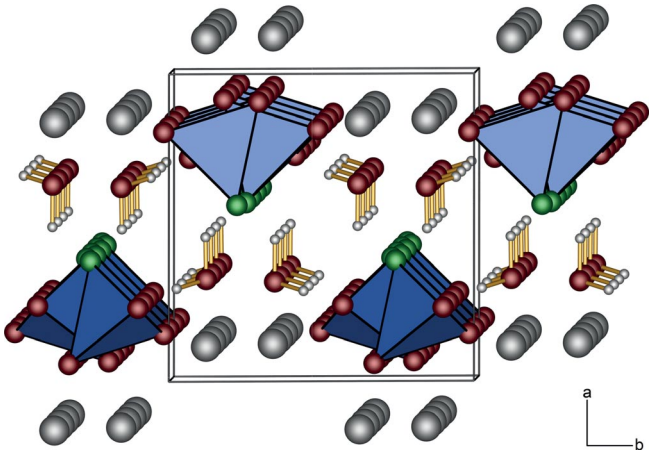

Figure 1. The crystal structure of $Sr(PO_3F)\cdot H_2O$ viewed along [001]; strontium grey, oxygen red, fluorine green, hydrogen white; the $(PO_3F)^{2-}$ ions are drawn as closed tetrahedra.

The Sr^{2+} ions are eightfold-coordinated by oxygen atoms only, two of which stem from water molecules (OW), and the remaining six originate from five PO_3F tetrahedra. The Sr–O bond lengths range from 2.48 to 2.82 Å, and the Sr–OW bond lengths lie between 2.58 and 3.00 Å. The average Sr–O bond length of 2.67 Å is in excellent agreement with the sum of the effective ionic radii of 2.64 Å.[18] The resulting $[SrO_8]$ polyhedron might be described as a snub disphenoid (Johnson polyhedron J_{50}), as shown in Figures 2 and S6 (Supporting Information). The oxygen and fluorine atoms in the $(PO_3F)^{2-}$ anion are well-ordered. The P–F bond is significantly longer than the P–O bonds, and the O–P–O angles are slightly larger than the O–P–F angles. Selected interatomic distances and angles of **1** are listed in Table 1. These are typical values for PO_3F tetrahedra and match those determined for related monofluorophosphates.[2,10,12,19] A compilation of the lengths of the longest P–F and the longest P–O bonds in numerous other fluorophosphate structures with metal or organic countercations was given recently.[20] The deviation of the PO_3F moiety in $Sr(PO_3F)\cdot H_2O$ from an ideal tetrahedron is very small (–0.4 %) and was calculated by applying the method suggested by Balic–Žunic and Makovicky on the basis that the positions of all experimentally determined ligands are enclosed by a sphere leading to an idealised tetrahedron's volume, which is then compared with the experimentally determined volume.[21,22] A short description of the method has been given previously.[8]

A distinct feature of the crystal structure of $Sr(PO_3F)\cdot H_2O$ is its layered character. The $[SrO_8]$ polyhedra share edges and corners to form sheets parallel to (100), and the $(PO_3F)^{2-}$ anions are attached below and above these sheets. The fluorine atoms of the PO_3F tetrahedra point towards the interlayer space. Adjacent sheets are held together by hydrogen bonds between water molecules and the oxygen and fluorine atoms of the PO_3F unit. The distances between the donors (D) and the oxygen and fluorine atoms as acceptor (A) atoms range between 2.7 and 3.0 Å (Table 2) and, hence, point to the possible formation of medium–strong H···F or H···O hydrogen bonds; however, the corresponding O–H···F angles are below 110°, which makes a significant interaction between water and fluorine relatively unlikely.[23,24] Consequently, the adhesion of the layers seems to be entirely dominated by O–H···O hydrogen bonds. This observation follows a general trend that hydrogen bonds of the type O–H···F do not play a significant role in water- or OH-containing

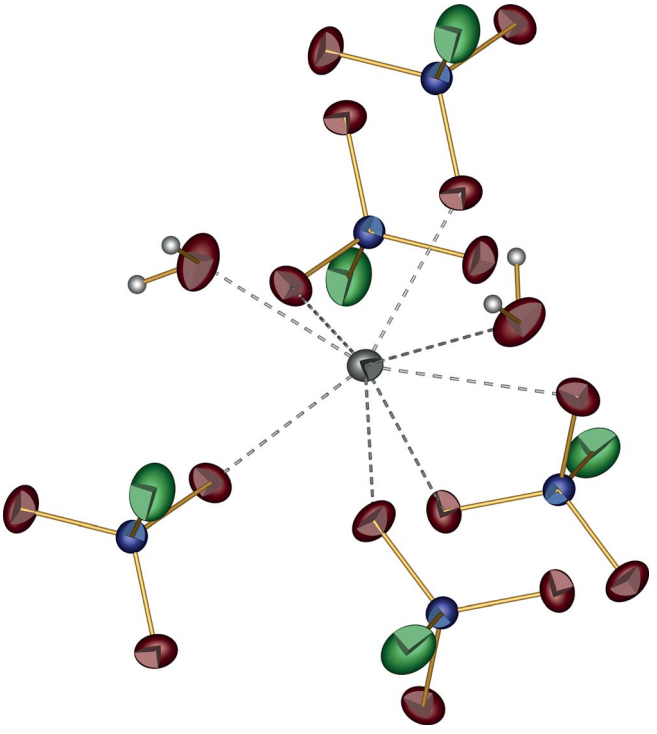

Figure 2. Coordination environment of the Sr^{2+} ions in $Sr(PO_3F)\cdot H_2O$ (the colour scheme is the same as that used in Figure 1); all non-H atoms are drawn with their displacement ellipsoids at a 75 % probability level.

Table 1. Relevant ranges of interatomic distances [Å] and angles [°] in $Sr(PO_3F)\cdot H_2O$ and $Sr(PO_3F)$ [the estimated standard deviations (esds) are in parentheses].

	$Sr(PO_3F)\cdot H_2O$	$Sr(PO_3F)$
Sr–O	2.4828(11)–2.8202(11)	2.515(4)–2.944(4)
Sr–OW	2.5752(11)–3.0039(13)	–
Sr–F	–	2.683(3)–2.869(4)
P–O	1.4945(11)–1.5186(11)	1.528(5)–1.539(4)
P–F	1.5801(9)	1.576(3)
O–P–O	110.21(6)–116.13(7)	110.2(4)–117.5(5)
O–P–F	103.90(6)–105.53(6)	101.3(3)–110.2(3)

Table 2. Possible hydrogen bonds in $Sr(PO_3F)\cdot H_2O$; D = donor, A = acceptor.

D–H	A	*d*(D–H) [Å]	*d*(H–A) [Å]	∠DHA [°]	*d*(D–A) [Å]
OW–H1	O3	0.95	1.92	141	2.717
OW–H2	O2	0.97	1.91	166	2.863
OW–H2	F	0.97	2.31	108	2.771
OW–H2	F	0.97	2.48	110	2.953

fluorophosphates.[25–29] Overall, one has to consider that the positions of the hydrogen atoms determined by the X-ray diffraction analysis are somewhat uncertain; therefore, only a highly probable scenario is suggested in this discussion.

Synthesis of $Sr(PO_3F)$

Unlike the previously mentioned monothiophosphates $NaM(PO_3S)\cdot 9H_2O$ (M = Mg, Ca, Sr,[7,30] Ba), which decompose by the loss of H_2S upon mild heating, $Sr(PO_3F)\cdot H_2O$ dehydrates without the evaporation of HF to yield phase-pure $Sr(PO_3F)$ above 80 °C. In a previous investigation on the thermal behaviour of $Sr(PO_3F)\cdot H_2O$, it was shown by simultaneous thermogravimetry and mass-spectroscopic measurements that the decomposition of the hydrous phase follows a multistage mechanism until the end-products α-$Sr_2P_2O_7$ and the apatite-type phase $Sr_5(PO_4)_3F$ form above 750 °C.[16] For the intrinsic dehydration, the authors determined a decomposition range of 80–140 °C and a mass loss corresponding to ca. 0.8 mol of water under the chosen conditions (heating range 10 °C/min, flowing Ar atmosphere). Both the previously reported decomposition range and the partial dehydration were confirmed by our observations. However, the dehydration of $Sr(PO_3F)\cdot H_2O$ itself appears not to follow a simple one-step mechanism. Differential scanning calorimetry (DSC) measurements revealed at least four well-resolved endothermic effects that accompany the loss of water in the temperature range 80–140 °C (Figure S1). Whether this multistage mechanism points to a stepwise (partial) dehydration or accompanying structural rearrangements or both could not be resolved with our experimental methods. The dehydration seems to be controlled kinetically and can be monitored at different heating rates and heating times of the samples. A partial dehydration occurs if the material is heated quickly or only for a short time above the onset of the dehydration temperature (as in the previous thermogravimetric study[16] or for the preparation of samples for solid-state NMR studies, see below), whereas slow heating rates and the retention of the chosen temperature for several hours or even days lead to complete dehydration. The differential weighing of a hydrous sample treated at 115 °C for two weeks under atmospheric conditions revealed a dehydration degree of more than 99 %. This sample did not contain any remaining crystal water as evidenced by infrared spectroscopy. The as-prepared $Sr(PO_3F)$ material is stable for at least five months when stored under ambient conditions, as shown by repeated powder X-ray diffraction measurements.

Crystal Structure of $Sr(PO_3F)$

The crystal structure of the anhydrous phase was solved from the X-ray powder diffraction data by simulated annealing; the resulting structure model was refined by the Rietveld method (Figure 3). $Sr(PO_3F)$ (**2**) crystallises in the monoclinic space group $P2_1/c$ with all atoms occupying general Wyckoff sites 4*e* and adopts a monazite-type crystal structure.[31] This is in contrast to the assumption that fluorophosphates are isotypic to the corresponding isoelectronic sulfates,[13,32] as $SrSO_4$ (celestine) crystallises isotypically with baryte in the space group *Pbnm*.

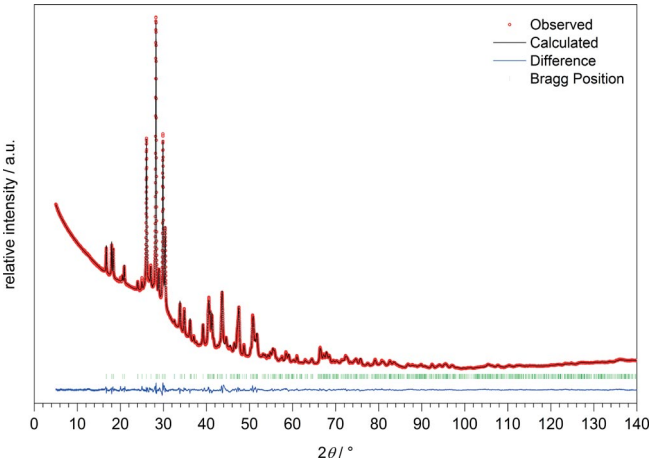

Figure 3. Observed (circles) and calculated (line) X-ray powder diffraction pattern (Cu-K_α radiation) as well as the difference profile of the Rietveld refinement of $Sr(PO_3F)$; the row of vertical lines indicates the possible peak positions of $Sr(PO_3F)$.

The close similarities between the crystal structures of the hydrous and anhydrous strontium fluorophosphates point towards a topotactic dehydration reaction, and this situation resembles the dehydration of layered $SrTeO_3\cdot H_2O$ to yield the framework structure of ε-$SrTeO_3$.[33]

In $Sr(PO_3F)$, the formerly layered arrangement of $Sr(PO_3F)\cdot H_2O$ transforms into a framework structure owing to the removal of water molecules. The similarities between both become apparent through the observation of the similar lattice parameters *b* and *c* in the two structures, the same type of zigzag chains of strontium cations (Sr–Sr distance 4.62 Å) and the same alignment of the PO_3F tetrahedra (P–P distance 4.59 Å) in an up-and-down orientation parallel to [001] in **2** (Figure 4).

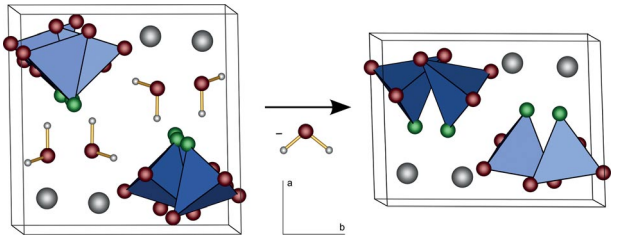

Figure 4. Representation of the crystal structures of $Sr(PO_3F)\cdot H_2O$ (left) and $Sr(PO_3F)$ (right) viewed along [001] (the colour scheme is the same as that used in Figure 1); with the loss of H_2O during dehydration, *a* shrinks significantly, whereas *b* and *c* change only slightly; the shown coordinate system applies for both unit cells.

The collapse of the crystal structure of **1** along [100] is reflected in drastic changes to *a* (change of 0.77 Å) and the monoclinic angle (change of 19.3°). During the dehydration, the PO_3F tetrahedra are tilted with respect to the strontium cation, the coordination number of which changes from eight to nine in the anhydrous phase. The resultant coordination polyhedron is a distorted triaugmented triangular prism composed of seven oxygen atoms and two fluorine atoms (Johnson polyhedron

J_{51}). Five PO_3F tetrahedra act as monodentate ligands through oxygen or fluorine atoms, and two act as bidentate ligands through oxygen and fluorine atoms (Figure 5 and Figure S6 in the Supporting Information).

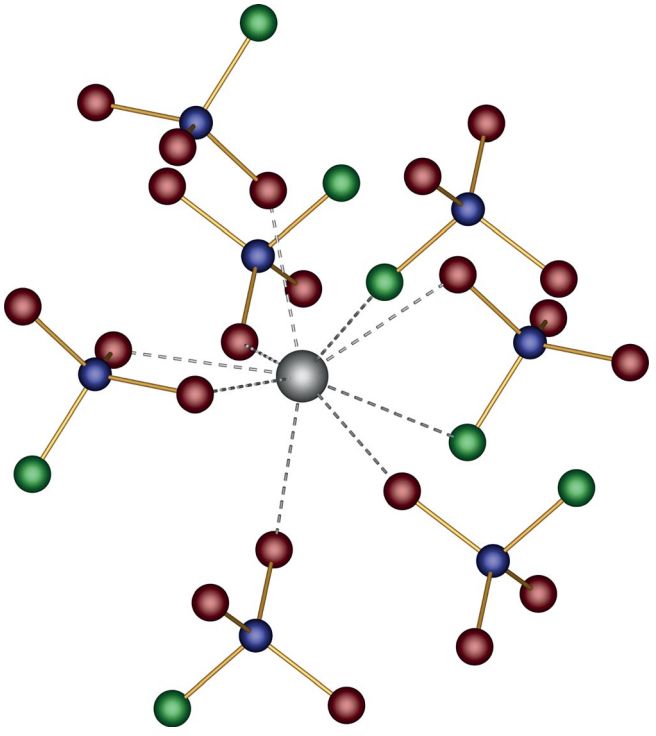

Figure 5. The coordination environment of the strontium ions in the crystal structure of $Sr(PO_3F)$; the colour scheme is the same as that used in Figure 1.

The Sr–O bond lengths range from 2.52–2.94 Å, and the Sr–F bond lengths range from 2.68 to 2.87 Å. The average coordination distances of 2.78 Å for the Sr–F bonds and 2.62 Å for the Sr–O bonds are in reasonable agreement with the sum of the effective ionic radii[18] of 2.64 Å for Sr–O and 2.62 Å for Sr–F bonds.

The PO_3F tetrahedron in the anhydrous phase shows basically the same features as that in the hydrous phase. The P–F bond length is longer than the average P–O bond length (1.58 vs. 1.53 Å), and the O–P–O angles are larger than the O–P–F angles. The deviation from an ideal tetrahedron in **2** is somewhat larger than that in **1** and amounts to –1.3 %. However, this larger deviation is presumably caused by the less accurate structure determination from powder diffraction data rather than by structural reasons. Selected interatomic distances and angles of $Sr(PO_3F)$ are listed in Table 1.

Electrostatic Calculations

We checked our structure model of $Sr(PO_3F)$ for electrostatic reasonability by using calculations based on the MAPLE concept.[37–39] A structure model is considered as electrostatically consistent if the sum of the MAPLE values of chemically similar compounds deviates from the MAPLE value of the compound of interest by less than 1 %. According to our calculations, the structure model shows electrostatic consistency (Table 3). Moreover, calculations with different assignments of the fluorine and oxygen atoms in the PO_3F unit yielded significantly larger deviations and, thus, confirmed the O/F ordering of our structure model.

Table 3. Result of the MAPLE calculations for $Sr(PO_3F)$ compared with those for SrO (ICSD no. 109461),[34] P_2O_5 (ICSD no. 40865),[35] and SrF_2 (ICSD no. 40414).[36]

MAPLE ($SrPO_3F$)	24703 kJ/mol
MAPLE (SrO)	3762 kJ/mol
MAPLE (P_2O_5)	42887 kJ/mol
MAPLE (SrF_2)	2790 kJ/mol
1/2 MAPLE (SrO + P_2O_5 + SrF_2)	24719.5 kJ/mol
Δ	0.1 %

Solid-State NMR Spectroscopy

To verify the presence of P–F bonds as well as the O/F ordering experimentally, ^{19}F and ^{31}P solid-state magic-angle spinning (MAS) NMR spectra were recorded. For ^{19}F–^{31}P bonds, the signals in the ^{19}F and ^{31}P spectra should be split into doublets as a consequence of the $^1J_{P,F}$ coupling. The ^{31}P MAS NMR spectra for both title compounds are shown in Figure 6. For $Sr(PO_3F)\cdot H_2O$ (Figure 6, upper spectrum), a doublet centred at $\delta \approx -3.4$ ppm with a $^1J_{P,F}$ coupling of (890 ± 10) Hz is observed, whereas the spectrum of $SrPO_3F$ (Figure 6, lower spectrum) comprises a doublet [$^1J_{P,F}$ = (840 ± 10) Hz] centred at $\delta \approx -2.1$ ppm. The spectra were recorded with the cross-polarisation (CP) of the ^{31}P nuclei in a $^{31}P\{^{19}F\}$ CPMAS NMR experiment without ^{19}F decoupling during acquisition. We note that the single-pulse acquisition spectra exhibit the presence of some minor phosphorus-containing impurities (phosphates); however, the cross-polarisation of ^{31}P from ^{19}F produces spectra in which only those ^{31}P species with direct proximity to ^{19}F nuclei contribute. Thus, the spectra confirm the presence of only one phosphorus position in each compound. The observed values for $^1J_{P,F}$ are typical for monofluorophosphates[2,11,40,41] and show the presence of only one phosphorus position in each

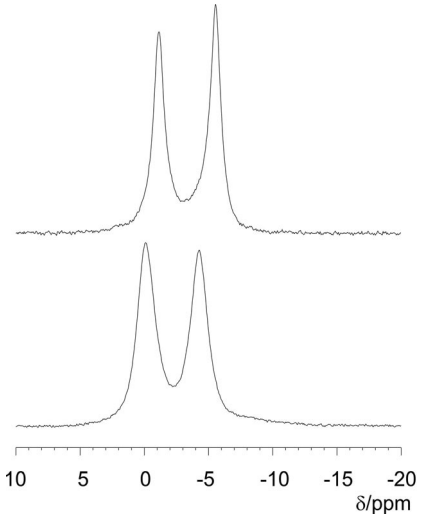

Figure 6. $^{31}P\{^{19}F\}$ CPMAS NMR spectra (no ^{19}F decoupling) for $Sr(PO_3F)\cdot H_2O$ (top) and $SrPO_3F$ (bottom).

compound. The ^{19}F MAS NMR spectra (not shown) also confirm the presence of PO_3F anions in both compounds. Here, we find doublets centred at δ = –70.0 pm [$^1J_{F,P}$ = (880 ± 20) Hz] for **1** and a signal at δ = –64.5 ppm [$^1J_{F,P}$ = (840 ± 20) Hz] for **2**.

The downfield shift by 5.5 ppm for **2** indicates a lower electron density around the F atom. This is in accordance with the coordination to the Sr^{2+} ion in **2** instead of the H^+ ion in **1**. In both spectra, an additional broad signal at $\delta \approx$ –87 ppm is observed. The observed chemical shift and the considerable line width indicate the presence of small amounts of SrF_2 (δ_{iso} = –84.5 ppm, strong ^{19}F–^{19}F dipolar interactions)[42] not detectable by powder XRD.

Vibrational Spectroscopy

The attenuated total reflectance (ATR) IR spectra of **1** and **2** are well-resolved (Figure 7) and show similar patterns, although some of the bands in the spectrum of the anhydrous material present additional splittings, which suggest the presence of correlation field effects. The broad bands in the region $\tilde{\nu}$ = 3600–3100 cm^{-1} and $\tilde{\nu} \approx$ 1660 cm^{-1} can be assigned to the OH valence and deformation vibrations in **1**, and these bands are absent in the spectrum of **2**.

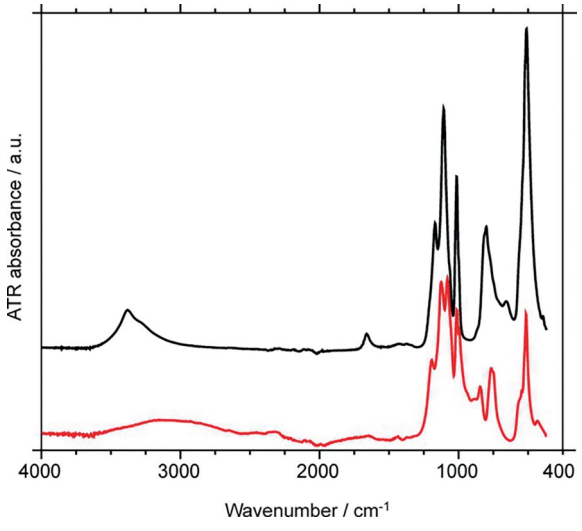

Figure 7. ATR infrared spectra of $Sr(PO_3F)\cdot H_2O$ (black) and $Sr(PO_3F)$ (red; dried in air at 115 °C for two weeks).

The Raman spectrum of $Sr(PO_3F)\cdot H_2O$ (Figure 8) is also well-resolved, whereas that of the anhydrous fluorophosphate is poorly resolved (Figure S2) owing to very high background fluorescence and was, therefore, not useful for this analysis.

Taking into account the mentioned characteristics of the $Sr(PO_3F)$ spectra, it appears useful to perform an initial factor-group analysis of the investigated lattices[43–45] on the basis of the known structural data and to correlate the symmetry of the "free" $(PO_3F)^{2-}$ anion (C_{3v}) with its site symmetry (C_1) and factor group (C_{2h}). The results of this correlation are shown in Table 4, and it becomes evident that the three doubly degenerate *E* modes are split under site-symmetry conditions, and all vibrations present IR and Raman activities. Furthermore, under factor-group symmetry, additional splittings are predicted, and the exclusion principle becomes operative, as the IR and Raman active modes belong to phonons of different parity.

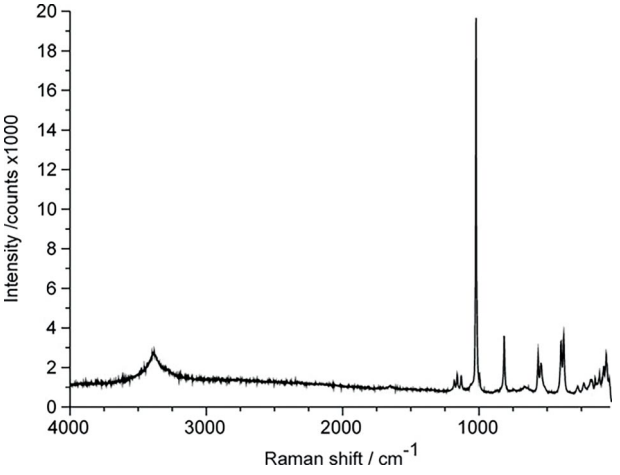

Figure 8. Raman spectrum of $Sr(PO_3F)\cdot H_2O$.

Table 4. Factor-group analysis of the $(PO_3F)^{2-}$ vibrations of the two investigated strontium monofluorophosphates.[a]

	Vibrational mode	Free anion (C_{3v})	Site symmetry (C_1)	Factor group (C_{2h})
ν_1	ν(P–F)	A_1	A	$A_g+B_g+A_u+B_u$
ν_2	$\nu_s(PO_3)$	A_1	A	$A_g+B_g+A_u+B_u$
ν_3	$\delta(FPO_3)$	A_1	A	$A_g+B_g+A_u+B_u$
ν_4	$\nu_{as}(PO_3)$	E	2A	$2A_g+2B_g+2A_u+2B_u$
ν_5	$\delta(PO_3)$	E	2A	$2A_g+2B_g+2A_u+2B_u$
ν_6	$\varrho(PO_3)$	E	2A	$2A_g+2B_g+2A_u+2B_u$

[a] Activity: free anion: A_1 and E: IR and Raman; site symmetry: A: IR and Raman; factor group: A_g, B_g: Raman; A_u, B_u: IR.

The simplicity of the vibrational spectra of **1** and **2** suggests that no significant correlation field effects operate in these cases; therefore, the spectroscopic analysis can be performed on the basis of the site-symmetry approximation, and the proposed assignment is shown in Table 5.

Table 5. Assignment of the vibrational spectra of $Sr(PO_3F)\cdot H_2O$ and $Sr(PO_3F)$; band positions given in cm^{-1} units.

Infrared	Raman	Assignment
$Sr(PO_3F)\cdot H_2O$		
3380 (vs), 3270 (sh)	3381 (w)	ν(OH)
1660 (w)	1647 (vw)	$\delta(H_2O)$
1168 (m), 1106 (vs)	1181(vw), 1160 (w), 1130 (w)	ν_4, $\nu_{as}(PO_3)$
1013 (s)	1022 (vs), 997 (w)	ν_2, $\nu_s(PO_3)$
801 (s)	816 (m)	ν_1, ν(P–F)
657 (w)	668 (vw)	see text
512 (vs)	567 (w), 545 (w)	ν_5, $\delta(PO_3)$
	399 (w), 380 (w)	ν_6, $\varrho(PO_3)$
$Sr(PO_3F)$		
1192 (m), 1125 (vs), 1080 (vs)		ν_4, $\nu_{as}(PO_3)$
1011 (vs), 995 (sh)		ν_2, $\nu_s(PO_3)$
844 (w), 749 (m)		ν_1, ν(P–F)
564 (sh), 546 (sh), 514 (s)		ν_5, $\delta(PO_3)$
434 (w)		ν_3, $\delta(FPO_3)$

Regarding the vibrations of the water molecules, the O–H stretching modes are seen as a unique relatively strong band

with a weak shoulder on the lower-energy side. The position of these bands is characteristic for the presence of hydrogen bridges of medium strength[46] and correlates[47] very well with the lengths determined for the hydrogen bonds in this structure (Table 2).

In agreement with the predictions of the site-symmetry analysis, the antisymmetric $\nu(PO_3)$ vibration presents two clear IR components. In the Raman spectrum, three relatively weak signals are observed in this region; this suggests the presence of weak correlation field effects in this case. The corresponding symmetric stretching vibration is the strongest Raman band and is accompanied by a very weak satellite band; this band is also relatively strong in the IR spectrum.

The ν(P–F) vibration can be clearly identified in both spectra at a slightly higher energy than that observed in the respective solution Raman spectrum ($\tilde{\nu}$ = 795 cm^{-1}).[46] The different position of the ν(P–F) bands at somewhat lower wavenumbers for **2** can be explained by the coordination of a F^- ion to a Sr^{2+} ion, which only occurs in **2** (Sr–F 3.32–3.52 Å in **1**, Sr–F 2.68–2.87 Å in **2**). Hence, the P–F bond strength is reduced in **2**, and the ν(P–F) vibration can be excited at lower energies.

The very weak IR band at $\tilde{\nu}$ = 657 cm^{-1} with a very weak Raman counterpart at $\tilde{\nu}$ = 668 cm^{-1} is probably a combination band. For the deformational modes, only $\delta(PO_3)$ could be identified as a very intense but unique IR band; in the Raman spectrum, this band is found as a clearly split vibration at somewhat higher wavenumbers, as predicted (cf. Table 4). No signals for the $\delta(FPO_3)$ mode could be found. In the Raman spectrum of a $(PO_3F)^{2-}$ solution, both vibrations are reported at the same energy ($\tilde{\nu}$ = 520 cm^{-1}),[46] although both vibrations were identified at slightly different wavenumbers for crystalline $Hg_2(PO_3F)$ with $\nu_5 > \nu_3$.[41] The corresponding ν_6 PO_3 rocking mode was identified as a very weak doublet in the Raman spectrum only.

The proposed assignment for the IR spectrum of $Sr(PO_3F)$ is presented in Table 5. The two $\nu(PO_3)$ vibrations are clearly split; for the antisymmetric mode, three of the four factor-group-predicted vibrations ($2A_u+2B_u$) are observed, whereas the two expected components (A_u+B_u) are seen for the symmetric mode.

In the poorly defined Raman spectra (Figure S2), only a weak doublet with components at $\tilde{\nu}$ = 1015 and 996 cm^{-1} can be observed. These bands clearly represent the two expected components (A_g+B_g) of the $\nu_s(PO_3)$ mode. As expected, the ν(P–F) vibration is also seen as a well-defined doublet, and the mean value of the observed components practically coincides with the solution value measured by Raman spectroscopy ($\tilde{\nu}$ = 795 cm^{-1}).[46]

In this case, we have again assigned $\nu_5 > \nu_3$, and this last vibration has been tentatively assigned to the weak feature at $\tilde{\nu}$ = 434 cm^{-1}. The vibrational mode ν_5 is found as a single strong band with two weak shoulders on the higher-energy side, that is, three of the four predicted components ($2A_u+2B_u$) are observed.

In summary, the observed vibrational spectroscopic behaviour of **1** is in good agreement with the site-symmetry predictions, although evidence for the presence of correlation field effects is observed in some spectral regions. These effects also become evident through the fact that small energy differences are always observed between the corresponding IR and Raman bands. Such differences are considered as a valuable criterion for the evaluation of the strength of the coupling effects in crystal structures[48,49] and confirm that they are relatively weak in the present case. For **2**, the correlation field effects are more evident from the spectroscopic behaviour; although the factor predictions are not totally fulfilled, significant splitting is generally observed for all infrared bands.

Conclusions

The crystal structures of $Sr(PO_3F)\cdot H_2O$ and the monazite-type $Sr(PO_3F)$ were determined by single-crystal and powder X-ray diffraction, respectively. The structural changes during the topotactic dehydration of the hydrous phase were followed by complementary spectroscopic methods (MAS NMR and vibrational spectroscopy), and DSC measurements showed very good agreement with the structural data. The very intense fluorescence of anhydrous $Sr(PO_3F)$, possibly caused by defects generated during the dehydration, and the concomitant very low resolution of the Raman spectra recorded at the red and blue laser lines did not allow a reasonable assignment of the corresponding Raman bands. As such a strong fluorescence was not observed in the Raman spectrum of $Sr(PO_3F)\cdot H_2O$, the change of the coordination environment of the Sr^{2+} ion from coordination number eight and an all-oxygen environment to coordination number nine with two fluorine ligands seems to have a crucial influence and makes $Sr(PO_3F)$ a promising host for phosphor materials. Systematic studies to incorporate different dopants and dopant concentrations in the $Sr(PO_3F)$ structure are underway.

Experimental Section

Synthesis of Polycrystalline $Sr(PO_3F)\cdot H_2O$: Polycrystalline $Sr(PO_3F)\cdot H_2O$ was synthesised in aqueous solution by metathesis. $Na_2(PO_3F)$ (200 mg, 1.39 mmol, Aldrich, purity 95 %) was dissolved in water (ca. 7 mL), and a solution of $Sr(NO_3)_2$ (294 mg, 1.39 mmol, Fluka, ≥99 %) or $SrCl_2\cdot 6H_2O$ (371 mg, 1.39 mmol, Aldrich, 99 %) in water (ca. 7 mL) was added dropwise. The colourless product precipitated upon the addition of acetone (ca. 100 mL, VWR, technical grade) and was collected by filtration (yield ca. 89 %). Alternatively, $(NH_4)_2(PO_3F)\cdot H_2O$ (prepared according to ref.[50]) can be used as the fluorophosphate source. The addition of concentrated aqueous $SrCl_2$ or $Sr(NO_3)_2$ solutions to a concentrated $(NH_4)_2(PO_3F)$ solution also affords the direct precipitation of $Sr(PO_3F)\cdot H_2O$. All reactions were performed in polytetrafluoroethylene (PTFE) beakers. The purity of the freshly prepared product was checked by powder X-ray diffraction. The observed intensities were in very good agreement with the diffraction pattern calculated from the single-crystal data (Figure S3).

Growth of $Sr(PO_3F)\cdot H_2O$ Single Crystals: To obtain single crystals, two crystal-growth procedures were employed. Firstly, the reaction was performed as described above; however, instead of fast precipitation through the addition of acetone, the solution was allowed to evaporate overnight in a desiccator with silica gel as a drying agent, and a few block-shaped colourless crystals were obtained. Secondly, $Ag_2(PO_3F)$[10] was initially dissolved in water. To this solution, the stoichiometric amount of an aqueous $SrCl_2$ solution was added. The

precipitated AgCl was removed by filtration, and the resulting solution was left to evaporate to dryness under ambient conditions over several days; again, block-shaped colourless crystals could be isolated.

Synthesis of $Sr(PO_3F)$: Polycrystalline $Sr(PO_3F)$ was obtained by dehydration of $Sr(PO_3F)\cdot H_2O$ in air at 80–115 °C in a compartment dryer. This method yielded $Sr(PO_3F)$ of poor crystallinity. Through very slow heating during a temperature-dependent X-ray powder diffraction measurement, we obtained a sample of much higher crystallinity (Figure S4) that was suitable for structure determination and subsequent Rietveld analysis (Figure 3). A Hilgenberg glass capillary was filled with finely ground $Sr(PO_3F)\cdot H_2O$ and mounted on a Bruker D8 Advance powder diffractometer equipped with a furnace. The sample was heated at 0.1 °C/s to the desired temperature and held there for 3 h, during which a diffraction pattern was acquired; this procedure was repeated every 5 °C between 47 and 117 °C (Figure S5).

Crystal-Structure Determination: The single-crystal X-ray diffraction data were collected at room temperature with a Bruker D8 Advance diffractometer equipped with a SMART APEXII 4k CCD detector by using Ag-K_α radiation; the data were corrected for absorption by applying a multiscan approach. The crystal structure of $Sr(PO_3F)\cdot H_2O$ was solved by direct methods with the SHELXTL program package[51] and refined with anisotropic displacement parameters for all non-H atoms; the F and O atoms could be distinguished through the different bond lengths within the PO_3F tetrahedron, in analogy with previously determined fluorophosphates structures. All hydrogen atoms were located by difference Fourier syntheses and refined isotropically with fixed $U_{iso} = 0.03$ Å^2 and restrained O–H distances of 0.99(1) Å. The details of the X-ray data collection are summarised in Table 6. The positional and displacement parameters for all atoms are listed in the Supporting Information (Tables S1 and S2).

Table 6. Crystal data and details of structure refinements.

	$Sr(PO_3F)\cdot H_2O$	$Sr(PO_3F)$
T /K	293(2)	293(2)
M /g mol^{-1}	203.61	185.59
Crystal system	monoclinic	monoclinic
Space group, no.	$P2_1/c$, 14	$P2_1/c$, 14
a /Å	7.4844(2)	6.71689(9)
b /Å	7.0793(2)	7.11774(11)
c /Å	8.4265(2)	8.66997(13)
β /°	108.6960(10)	128.0063(7)
V /Å^3	422.913(19)	326.605(8)
Z	4	4
$\varrho_{X\text{-ray}}$ /g cm^{-3}	3.198	3.774
Crystal size/ mm^3	0.10 × 0.08 × 0.05	
Colour / shape	colourless block	
μ /mm^{-1}	7.054	
F(000)	384	
Radiation (λ /Å)	Ag-K_α (0.56087)	Cu-K_α
Diffractometer	Bruker D8 Advance	Bruker D8 Advance
Absorption correction	multiscan	
Min./max. transmission	0.8441/1.000	
Index range	–13/–12/–14–12/12/14	
Θ range /°	2.27–29.50	2.5–70.0
Collected reflections	28333	1278
Independent data/restraints/ parameters	2391/2 /70	33
Observed reflections ($I > 2\sigma$), R_{int}	1947, 0.045	47 background points
R (all data)	$R_1 = 0.036$	$R_p = 0.010$
	$wR_2 = 0.049$	$R_{wp} = 0.015$
	$w^{-1} = [\sigma^2(F_o^2) + (0.0224P)^2 + 0.1278P]$	$R_F = 0.030$
	$P = (F_o^2 + 2F_c^2)/3$	$R_{Bragg} = 0.038$
GooF	1.054	
Min./max. residual density /e Å^{-3}	–0.54/1.11	
χ^2		8.94

Powder X-ray Diffraction: The powder X-ray diffraction data were collected with a Bruker D8 Advance diffractometer equipped with a furnace and a capillary mounting system by using Cu-K_α radiation (LynxEye 1-D detector, steps of 0.2°, acquisition time 12–17 s/step, Soller slits 4°, fixed divergence slit 1 mm, transmission geometry). The generator was driven at 40 kV and 40 mA. The samples were finely ground and prepared in Hilgenberg glass capillaries (outer diameter 0.3 mm). The X-ray powder diffraction pattern of $Sr(PO_3F)$ was recorded in the 2θ range 5.0–140.0° with steps of 0.2° and an acquisition time of 17 s/step. Profile fitting and structure solution through simulated annealing were performed with EXPO2013.[52,53] The obtained structure model was refined with the program suite FullProf and the graphical user interface WINPlotR.[54] The results are summarised in Table 6 and shown in Figure 3. The atomic coordinates and their respective isotropic displacement parameters are listed in the Table S3.

Further details on the crystal structure investigations may be obtained from the Fachinformationszentrum Karlsruhe, 76344 Eggenstein-Leopoldshafen, Germany (fax: +49-7247-808-666; e-mail: crysdata@fiz-karlsruhe.de), on quoting the depository numbers CSD-429339 [$Sr(PO_3F)\cdot H_2O$] and -429338 [$Sr(PO_3F)$].

MAS NMR Spectroscopy: The ^{19}F and ^{31}P MAS NMR spectra were recorded with a Varian 500 NMR spectrometer with Larmor frequencies of 470.6 (^{19}F) and 202.3 MHz (^{31}P) at a spinning speed of 35 kHz and a Varian 1.6 mm MAS NMR probe. A $\pi/2$ pulse length of 2 (^{19}F) or 2.5 µs (^{31}P) was used. The ^{19}F spectra were referenced to $CFCl_3$, and the ^{31}P spectra were referenced to H_3PO_4. For the $^{31}P\{^{19}F\}$ CPMAS NMR experiment, contact times of 5 ms were employed. Relaxation delays of 1200–1800 s were used for the acquisition of the spectra.

Vibrational Spectroscopy: A Bruker Tensor 27 FTIR spectrometer combined with a Harrick MVP2 Series diamond ATR accessory was used to record spectra in the $\tilde{\nu}$ = 4000–370 cm^{-1} region. The Raman spectra were recorded with a Renishaw RM 1000 micro-Raman system in the spectral range $\tilde{\nu}$ = 4000–40 cm^{-1}. The 632.8 nm excitation line of a 17 mW HeNe laser was focused on the sample surface with a 50×/0.75 objective lens. The Raman intensities were collected with a thermoelectrically cooled CCD array detector. The resolution of the system was 4 cm^{-1}, the wavenumber accuracy was ±1 cm^{-1}, both calibrated with the Rayleigh line and the 520.5 cm^{-1} line of a Si standard. Owing to the very high fluorescence of anhydrous $Sr(PO_3F)$ under the red laser light, this sample was additionally measured with a blue laser in the spectral region $\tilde{\nu}$ = 1600–40 cm^{-1}, but a spectrum with similar very high fluorescence was obtained (Figure S2).

Differential Scanning Calorimetry (DSC): For the DSC measurements, a NETZSCH DSC 200 F3 Maia system was employed; aluminium pans with pierced lids were filled with the samples and heated at a heating rate of 2.5 °C/min in a flowing argon atmosphere (20 mL/min) in the temperature range 30–230 °C.

Acknowledgments

E. J. B. acknowledges the continuous support from the Universidad Nacional de La Plata. The authors thank Prof. Dr. Wolfgang Scherer (University of Augsburg, Germany) for the single-crystal data collection.

Keywords: Main group elements · Layered compounds · Solid-state structures · Structure elucidation · Topotactic reactions

[1] K. Kazmierczak, J. G. Heck, H. A. Höppe, *Z. Anorg. Allg. Chem.* **2010**, *636*, 409–413.
[2] B. Stöger, M. Weil, J. Skibsted, *Dalton Trans.* **2013**, *42*, 11672–11682.
[3] H. A. Höppe, M. Daub, O. Oeckler, *Solid State Sci.* **2009**, *11*, 1484–1488.
[4] H. A. Höppe, *Solid State Sci.* **2005**, *7*, 1209–1215.
[5] H. A. Höppe, *Z. Anorg. Allg. Chem.* **2005**, *631*, 1272–1276.
[6] H. A. Höppe, S. J. Sedlmaier, *Inorg. Chem.* **2007**, *46*, 3467–3474.
[7] H. A. Höppe, S. W. Scharinger, J. G. Heck, K. Kazmierczak, *Solid State Sci.*, article submitted.
[8] H. A. Höppe, *J. Solid State Chem.* **2009**, *182*, 1786–1791.
[9] R. G. Pearson, *Inorg. Chim. Acta* **1995**, *240*, 93–98.
[10] M. Weil, M. Puchberger, E. Füglein, E. J. Baran, J. Vannahme, H. J. Jakobsen, J. Skibsted, *Inorg. Chem.* **2007**, *46*, 801–808.
[11] M. Weil, M. Puchberger, E. J. Baran, *Inorg. Chem.* **2004**, *43*, 8330–8335.
[12] A. Perloff, *Acta Crystallogr., Sect. B* **1972**, *28*, 2183–2191.
[13] W. Lange, *Ber. Dtsch. Chem. Ges. B* **1929**, *62*, 793–801.
[14] V. Q. Kinh, G. Montel, *Compt. Rend.* **1961**, *252*, 3809–3811.
[15] V. Q. Kinh, *Dissertation*, Université de Paris, France, **1962**.
[16] D.-H. Menz, K. Heide, C. Kunert, C. Mensing, L. Kolditz, *Z. Anorg. Allg. Chem.* **1986**, *540/541*, 191–197.
[17] M. Rafiq, J. Durand, L. Cot, *C. R. Acad. Sci., Ser. IIc* **1979**, *288*, 411–413.
[18] R. D. Shannon, *Acta Crystallogr., Sect. A* **1976**, *32*, 751–767.
[19] J. Durand, L. Cot, M. Berraho, M. Rafiq, *Acta Crystallogr., Sect. C* **1987**, *43*, 611–613.
[20] J. Fábry, M. Fridrichová, M. Dušek, K. Fejfarová, R. Krupková, *Acta Crystallogr., Sect. C* **2012**, *68*, o76–o83.
[21] T. Balic-Žunic, E. Makovicky, *Acta Crystallogr., Sect. B* **1996**, *52*, 78–81.
[22] E. Makovicky, T. Balic-Žunic, *Acta Crystallogr., Sect. B* **1998**, *54*, 766–773.
[23] T. Steiner, *Angew. Chem. Int. Ed.* **2002**, *41*, 48–76; *Angew. Chem.* **2002**, *114*, 50.
[24] P. A. Wood, F. H. Allen, E. Pidcock, *CrystEngComm* **2009**, *11*, 1563–1571.
[25] H. A. Prescott, *Dissertation*, Humboldt University Berlin, Germany, **2001**.
[26] H. A. Prescott, S. I. Troyanov, E. Kemnitz, *Z. Anorg. Allg. Chem.* **2002**, *628*, 152–156.
[27] H. A. Prescott, S. I. Troyanov, M. Feist, E. Kemnitz, *Z. Anorg. Allg. Chem.* **2002**, *628*, 1749–1755.
[28] H. A. Prescott, S. I. Troyanov, E. Kemnitz, *Z. Kristallogr.* **2003**, *218*, 604–611.
[29] E. Kemnitz, H. A. Prescott, S. I. Troyanov, *Z. Kristallogr.* **2000**, *215*, 240–245.
[30] M. Gjikai, *Z. Kristallogr. New Cryst. Struct.* **2008**, *223*, 1–2.
[31] Y.-X. Ni, J. M. Hughes, A. N. Mariano, *Am. Mineral.* **1995**, *80*, 21–26.
[32] H. C. Goswami, *J. Indian Chem. Soc.* **1937**, *14*, 660–666.
[33] B. Stöger, M. Weil, E. J. Baran, A. C. Gonźalez-Baro, S. Malo, J. M. Rueff, S. Petit, M. B. Lepetit, B. Raveau, N. Barrier, *Dalton Trans.* **2011**, *40*, 5538–5548.
[34] J. Bashir, R. T. A. Khana, N. M. Butt, G. Heger, *Powder Diffr.* **2002**, *17*, 222–224.
[35] H. Arnold, *Z. Kristallogr.* **1986**, *177*, 139–142.
[36] J. B. Forsyth, C. C. Wilson, T. M. Sabine, *Acta Crystallogr., Sect. A* **1989**, *45*, 244–247.
[37] R. Hoppe, *Angew. Chem. Int. Ed. Engl.* **1966**, *5*, 95–106; *Angew. Chem.* **1966**, *78*, 52.
[38] R. Hoppe, *Angew. Chem. Int. Ed. Engl.* **1970**, *9*, 25–34; *Angew. Chem.* **1970**, *82*, 7.
[39] R. Hübenthal, *MAPLE, Program for the Calculation of the Madelung Part of Lattice Energy*, University of Gießen, Germany, **1993**.
[40] T. C. Farrar, J. L. Schwartz, S. Rodriguez, *J. Phys. Chem.* **1993**, *97*, 7201–7207.
[41] A.-R. Grimmer, K.-H. Jost, D. Müller, J. Neels, *J. Fluorine Chem.* **1987**, *34*, 347–360.
[42] B. Bureau, G. Silly, J. Y. Buzaré, J. Emery, *Chem. Phys.* **1999**, *249*, 89–104.
[43] S. D. Ross, *Inorganic Infrared and Raman Spectra*, McGraw Hill, London, **1972**.
[44] A. Müller, E. J. Baran, R. O. Carter, *Struct. Bonding (Berlin)* **1976**, *26*, 81.
[45] A. Fadini, F. M. Schnepel, *Vibrational Spectroscopy: Methods and Applications*, Ellis Horwood, Chichester, UK, **1989**.
[46] H. Siebert, *Anwendungen der Schwingungsspektroskopie in der Anorganischen Chemie*, Springer, Berlin, **1966**.
[47] E. Libowitzky, *Monatsh. Chem.* **1999**, *130*, 1047–1059.
[48] A. Müller, *Z. Naturforsch. A* **1966**, *21*, 433–436.
[49] E. J. Baran, E. G. Ferrer, I. Bueno, C. Parada, *J. Raman Spectrosc.* **1990**, *21*, 27–30.
[50] U. Schülke, R. Kayser, *Z. Anorg. Allg. Chem.* **1991**, *600*, 221–226.
[51] G. M. Sheldrick, *Acta Crystallogr., Sect. A* **2008**, *64*, 112–122.
[52] A. Altomare, M. Camalli, C. Cuocci, C. Giacovazzo, A. Moliterni, R. Rizzi, *J. Appl. Crystallogr.* **2009**, *42*, 1197–1202.
[53] A. Altomare, C. Cuocci, C. Giacovazzo, A. Moliterni, R. Rizzi, N. Corriero, A. Falcicchio, *J. Appl. Crystallogr.* **2013**, *46*, 1231–1235.
[54] J. Rodriguez-Carvajal, *Phys. B* **1993**, *192*, 55–69.

Received: October 3, 2015
Published Online: February 8, 2016

